THE ASTROPHYSICAL JOURNAL, 506:712–720, 1998 October 20

A NEARBY GALAXY IN THE DEEP-ULTRAVIOLET: *VOYAGER 2* OBSERVATIONS OF M33 FROM Lyα TO THE LYMAN LIMIT

WILLIAM C. KEEL
Department of Physics and Astronomy, University of Alabama, Box 870324, Tuscaloosa, AL 35487; keel@bildad.astr.ua.edu
Received 1998 February 18; accepted 1998 May 28

ABSTRACT

Observations of high-redshift galaxies in the emitted-wavelength regime around Lyα have renewed interest in the appearance of normal galaxies in the deep ultraviolet. This paper presents an analysis of spectrophotometry of the local Sc galaxy Messier 33 (NGC 598) obtained by *Voyager 2*, covering the range from below the Lyman limit to about 1250 Å. The scanning nature of the observation preserves one dimension of spatial resolution across the galaxy. M33 exhibits net Lyα emission at equivalent width $\approx$100 Å and observed flux $1.8 \pm 0.4 \times 10^{-9}$ ergs cm^{-2} s^{-1}. The line emission is broadly concentrated toward the center, but there is no peak coincident with the giant H II region NGC 604. This may suggest that Lyα photons from spirals escape preferentially from the diffuse interstellar medium rather than from individual luminous H II regions. The global Lyα/Hα ratio is at least 3. We must see Lyα at the radial velocity range of M33 through substantial structure in the foreground H I of the Milky Way, since applying the mean column density averaged over large scales would give negligible transmission. Therefore, the actual Lyα intensity must be larger than measured. The continuum shows the Lyβ/O VI/C II λ 1030 and Lyγ/C III λ 980 complexes in absorption and a decline in flux toward the Lyman limit. The dominant sources of radiation between 912 and 1216 Å are B stars, which is not surprising, since this is where their output peaks. The global spectrum declines only slightly in F_λ from 1500 to 1000 Å then declines sharply toward the Lyman limit. The intrinsic stellar spectrum must rise again shortward of the Lyman limit in order to match the intensity of recombination lines such as Hα. The spectrum is very well fitted by a weighted sum of B-star reference spectra, which would correspond to a current main-sequence mass function of $N(M) \propto M^{-4.7 \pm 0.3}$, although the important role of evolved B stars means that this fit does not necessarily correspond to the actual mass distribution. The stellar population in NGC 604 has bluer deep-UV colors than the rest of the galaxy, and the continuum in the *Voyager* passband follows the trend of flatter gradients for shorter wavelengths found from UV Imaging Telescope imagery. The continuum shape is a close match for that shown in Hopkins Ultraviolet Telescope observations of two starburst systems, as is expected from the short lifetimes of stars responsible for the deep-UV radiation. A simple comparison of the continuum and line properties of M33 with those of star-forming galaxies at high redshifts indicates that it is both fainter and much larger than the objects we can now detect in the early universe, pointing out how strongly our sample is (and will remain for some time) biased in favor of objects that are both compact and have absolutely high star formation rates. However, the detection of Lyα in M33, with nontrivial metallicity, bolsters the argument that many of the objects with such emission at high redshift are star-forming galaxies rather than those powered by active nuclei. The starburst system Mrk 357 at $z = 0.053$ has significant Lyα as well, from an archival *IUE* observation, providing a further example of such emission from star-forming systems. Tabulated properties are shown for nearby B stars observed with the UV Spectrometer systems on *Voyagers 1* and *2* used here as reference objects for crude spectral synthesis.

Subject headings: galaxies: individual (M33) — galaxies: photometry — ultraviolet: galaxies

1. INTRODUCTION

Recent work on high-redshift galaxies has focused attention on the ultraviolet spectra of galaxies in general and in particular on the need to understand the properties of nearby, well-understood systems at these wavelengths in order to enable a realistic interpretation of the wealth of data now emerging on galaxies at $z > 3$. The Lyman-dropout technique has proved to be a very reliable indicator of high-redshift systems, allowing Steidel et al. (1996a, 1996b, 1998) and Lowenthal et al. (1997) to obtain spectra of numerous galaxies whose Lyman limit is redshifted into the optical range. These galaxies show absorption features associated with hot stars (largely wind features), while Lyα may be in net emission or absorption. At somewhat smaller redshifts, Pascarelle et al. (1996) have identified a population of small, rather low-luminosity Lyα emitters that they conjecture are the premerger forerunners of today's more luminous systems.

The occurrence of Lyα emission in nearby galaxies has been a matter of some contention, with both the observational and theoretical situations remaining unsettled. Early predictions for the behavior of young galaxies called for enormous Lyα intensities, while the first *IUE* studies of star-forming galaxies showed little or no line radiation. Detailed consideration of the radiative transfer in a realistic interstellar medium suggested that resonant trapping of Lyα photons plays a crucial role (Bonilha et al. 1979); as indicated by the usual applicability of "Case B" recombination theory to H II regions, a Lyα photon is typically scattered many more times before escape than a neighboring continuum photon, giving a correspondingly higher probability of being absorbed by a grain than applies to the continuum, plus a significant probability of being degraded into photons in other recombination lines. These results seemed to suggest that Lyα emission, far from being a useful indicator of star formation, should be very weak in most galaxies.

Further *IUE* spectra by Hartmann et al. (1988) of star-forming galaxies with a range in metallicity, all distant enough for their redshifts to separate intrinsic from geocoronal Lyα, did provide some support for the notion that the equivalent width of Lyα emission might depend mostly on abundances (which could alter the grain population). However, reprocessing of an extensive set of *IUE* observations by Giavalisco, Koratkar, & Calzetti (1996a) showed no significant coupling of metallicity and Lyα strength, suggesting that structure in the galaxies' interstellar medium (ISM) is the dominant factor in the escape of Lyα photons. Most of these objects could be classified as starbursts; perhaps the most extreme one observed with *IUE* was Mrk 357 at $z = 0.053$, which shows emission at EW = 10 Å from the Final Archive spectrum. Recent *Hubble Space Telescope* (*HST*) spectroscopy has given mixed results (Lequeux et al. 1995; Thuan & Izotov 1997); neither abundances nor bulk velocity fields seem to explain which objects show emission (as large as EW = 70 Å in the small apertures used by *HST*) and which show only net absorption; it is especially noteworthy that the two most metal-poor galaxies known, I Zw 18 and SBS 0335−052, show only net absorption in Lyα (Kunth et al. 1994; Thuan & Izotov 1997). As Thuan & Izotov note, this raises the possibility of a strong role for the smaller scale structure of the ISM in whether significant numbers of Lyα photons escape star-forming galaxies.

The limited data available on nearby galaxies from *IUE* have left important questions unaddressed. Just how widespread is Lyα emission in "normal" galaxies, and where does it come from? Under what conditions do line photons manage to escape not only their generating environment but the whole galaxy? These issues are becoming important in comparing the local universe to what we find at high redshifts. The continuum behavior in the deep-UV, beyond *IUE*'s wavelength range, is also fresh ground for comparison. In this light, although currently difficult to obtain, deep-UV data on any well-understood local examples are very valuable.

The *Voyager*s have been literally in the best position to escape the effects of geocoronal Lyα emission. Their UV Spectrometers (UVSs) operate to the Lyman limit and beyond, making them a unique resource for bright enough UV targets. An examination of nearby galaxies in the UVS archives has turned up a unique spatially resolved observation of M33 obtained 20 years ago, which is finally reported and analyzed here.

2. DATA

2.1. *Voyager 2 Spectrophotometry*

M33 was well observed in a 5 day scan, conducted starting 1978 February 16 (flight day 47) and crossing the galaxy 2 days later, by the *Voyager 2* UVS. The UVS, as described by Broadfoot et al. (1977), covers the wavelength range from well below the Lyman limit to about 1675 Å, with the most useful sensitivity in the range shortward of Lyα. To minimize the effects of the poor reflectivity of most optical coatings at these wavelengths, the UVS employs no focusing foreoptics, defining its field of view with mechanical collimators. Light from a rectangular area of the sky 0°.10 × 0°.87 is dispersed and focused by a concave diffraction grating onto a microchannel plate and a 128 element readout array. The effective spatial and spectral resolutions are set for extended sources by the projection of the short axis of the admitting aperture (which I will call the "slit" for convenience if not precision) at 0°.05 spatially and ≈30 Å along the spectrum.

The *Voyager* instrument-pointing coordinate system is based on the Earth-spacecraft (high-gain antenna) axis, with the zero point in roll about this axis set by a bright reference star (Canopus for the early part of the *Voyager 2* mission). For the M33 observations, the UVS pointing was fixed in spacecraft coordinates and the slit was allowed to drift across the galaxy as the Sun-spacecraft vector swept across the sky, since the angular orbital motion was still slightly greater than 0°.5 per day at this point. Figure 1 shows the area covered, with slit positions at daily intervals nearest the time of crossing the center of M33. The long axis of the aperture ran along P.A. 163°, while the direction of motion was not quite perpendicular, in P.A. 63°. Each piece of the galaxy was observed for about 10,000 s. With an angular diameter of 71′ (to the $B = 25$ arcsec^{-2} isophote from the Third Reference Catalog [RC3] by de Vaucouleurs et al. 1991), M33 is large enough for structure to be resolved by the UVS slit.

The data handling and reduction used the suite of routines developed at the Lunar and Planetary Laboratory. Pointing corrections were derived to include the effects of spacecraft limit-cycle motion, so that all individual short data blocks could be combined on a consistent spatial scale. After binning by pointing direction (along the scan axis seen in Fig. 1), the wavelength-dependent background was subtracted by linear interpolation between regions well beyond the detected area of M33. Though the deep-UV sky background is quite dark, the relatively large field of view makes the UVS very sensitive to low surface brightness emission from both target objects and the (foreground) sky. The continuum skylight is mostly smooth and well behaved in space and time, so it can be well subtracted. However, the Lyman lines (of which α and β are detectable) do vary both spatially and temporally in response to solar activity (i.e., Sandel, Shemansky, & Broadfoot 1978). The behavior of Lyα is particularly important, since measuring this line in M33 is highly desirable. As a check on the reality of what appeared to be net Lyα emission associated with M33, the intensity of the He I λ584 line after similar background subtraction was examined, since the He I and H I lines from the interplanetary medium are found to vary closely in step (Shemansky, Sandel, & Broadfoot 1979). The scanning nature of the observations means that temporal changes in foreground emission, beyond the usual linear interpolation across the galaxy, can masquerade as spatial changes in Lyα, so an independent check for such changes is important. The maximum allowable scaled version of the He I temporal variation was subtracted from the Lyα profile, as shown in Figure 2, to give the most conservative interpretation as to the presence and strength of Lyα from M33. The final derived Lyα flux was modified to reflect this correction, reducing the flux by about 30% but still leaving a significant detection.

After background subtraction, instrumental scattered light was removed using an explicit descattering matrix transformation (having the net effect of deconvolving the

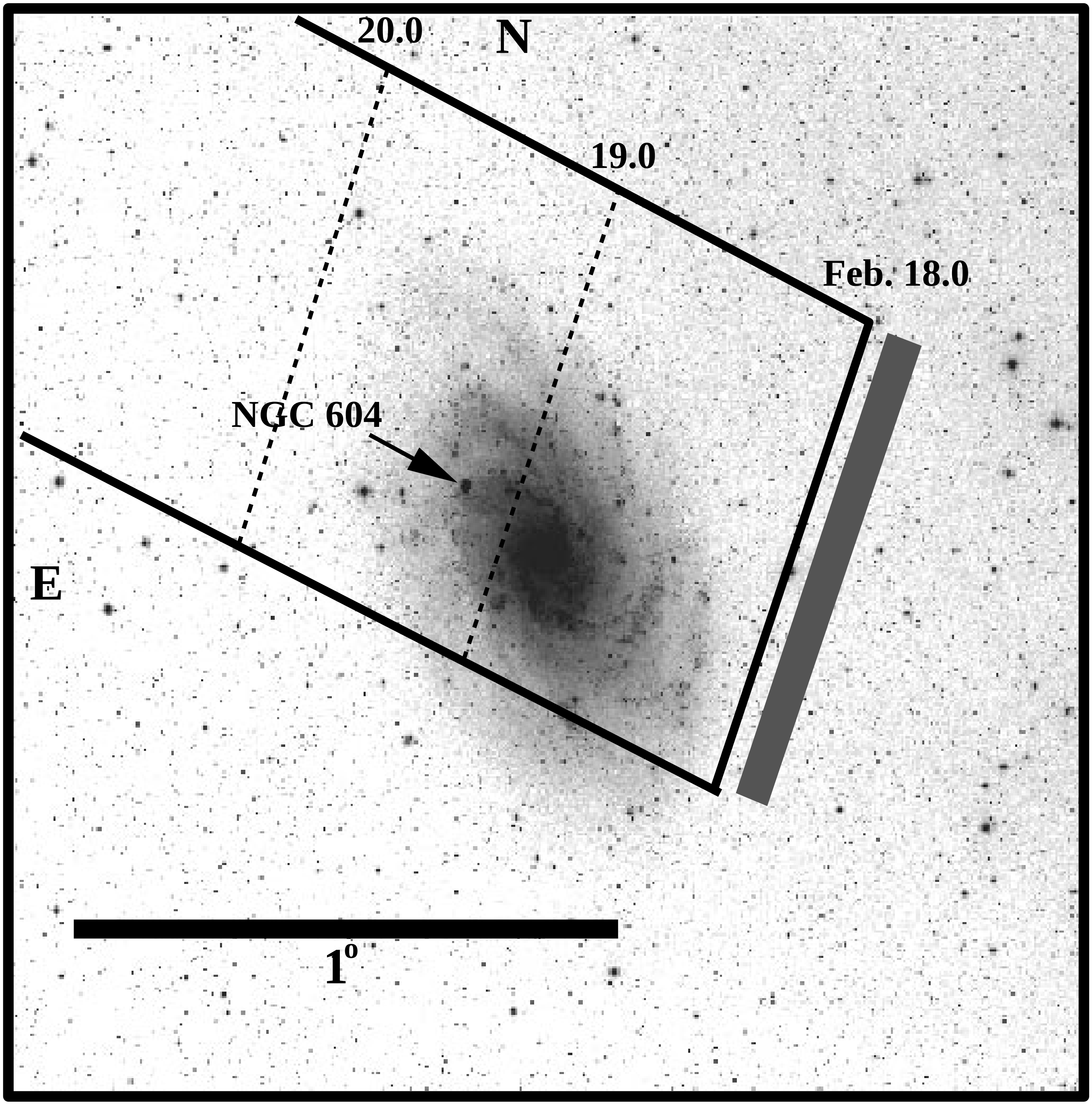

FIG. 1.—The trace of the UVS aperture across M33, superposed on a 2° region of the Digitized Sky Survey blue-light image. The angular extent and orientation of the entrance aperture are shown by the shaded rectangle, and its location is marked at 1 day intervals (at 0^h UT) as the spacecraft motion swept it across the galaxy. The dimension of spatial resolution in the M33 UVS spectrum is along the direction of motion, almost east-west.

pixel-to-pixel scattering). This results in an artificial spectral discontinuity just longward of Lyα at the edge of a coating applied to the long-wavelength part of the detector array. The affected pixel is ignored in the data presented here. The standard UVS intensity calibration was applied to place the extracted spectra on an absolute energy scale. For examination, spectra in $0\overset{\circ}{.}05$ bins were extracted spaced every $0\overset{\circ}{.}025$. The result is a calibrated "long-slit" spectrum of M33 extending from the Lyman limit to just longward of Lyα, with a spatial resolution of about $0\overset{\circ}{.}1$ and covering virtually the entire galaxy. The total detected count rate (object + background, usually dominated by background) was used to estimate the statistical error of each point in the spectrum.

The M33 spectrum may be corrected for foreground Galactic reddening, using the value $A_B = 0.18$ from the RC3 (de Vaucouleurs et al. 1991); while slightly higher values have been derived from multicolor photometry (Johnson & Joner 1987), the difference in the UV spectral shape is slight. *Voyager* observations of hot-star pairs, matched by spectral type, show that the Savage & Mathis (1979) analytic form is an adequate representation down to the Lyman limit (Longo et al 1989; Snow, Allen, & Polidan 1990). Thus, the UV spectrum was dereddened using the Savage & Mathis

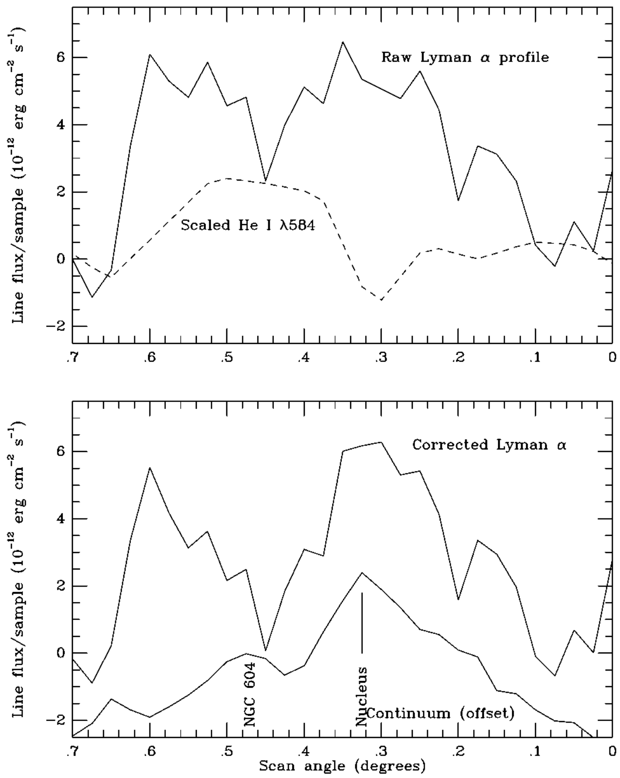

FIG. 2.—Spatial trace of Lyα emission and the use of He I λ584 emission to correct for possible residual temporal changes. The He I residual profile (following linear background subtraction from the ends of the scan) is scaled to match the Lyα residuals at its peak then subtracted to give the largest correction for artifacts due to confusing temporal changes in solar system emission with spatial changes across M33. The adopted Lyα profile after this correction is shown in the lower panel. For position reference, an offset trace of the continuum from 950 to 1150 Å is also shown, with the locations of the nucleus and NGC 604 marked. The intensity scale for the emission-line profiles is in flux per 0°.05 spatial bin, evaluated in overlapping bins at 0°.025 intervals.

curve scaled to the estimated foreground extinction at B. Effects of H_2 absorption bands (shortward of 1140 Å and strongest from 960–1030 Å) are less than 3% at any relevant wavelength, taking the typical foreground value for $N(\text{H I}) = 5.2 \times 10^{20}$ cm^{-2}, a representative value of $N(H_2)/N(\text{H I}) = 0.03$, and scaling from Figure 1 of Snow et al. (1990), so its effect could be safely ignored in these data. The integrated spectrum, as both observed and dereddened, is shown in Figure 3. For this modest data volume, it is also practical to tabulate the integrated spectrum (as observed before any foreground reddening correction), as in Table 1, that covers the range from 900 to 1300 Å over which the M33 data have useful signal-to-noise ratio. The units of flux are ergs cm^{-2} s^{-1} Å^{-1}, and the error is tabulated in units of 10^{-13} ergs cm^{-2} s^{-1} Å^{-1}.

Only foreground reddening has been corrected, for two reasons. First, with the aim of comparing the far-UV spectrum of M33 and high-redshift galaxies, only the differential effects of dust between the low- and high-redshift galaxies will remain, rather than uncertainties in the absolute effects at both ends of the scale. Second, and perhaps more fundamental, internal extinction effects are extremely difficult to evaluate. Balmer decrements show mean extinctions in giant H II regions of $A_V = 0.6$–0.8 mag (e.g., McCall, Rybski, & Shields 1985), with somewhat larger values in some parts of NGC 604 (Díaz et al. 1987). Even so, these

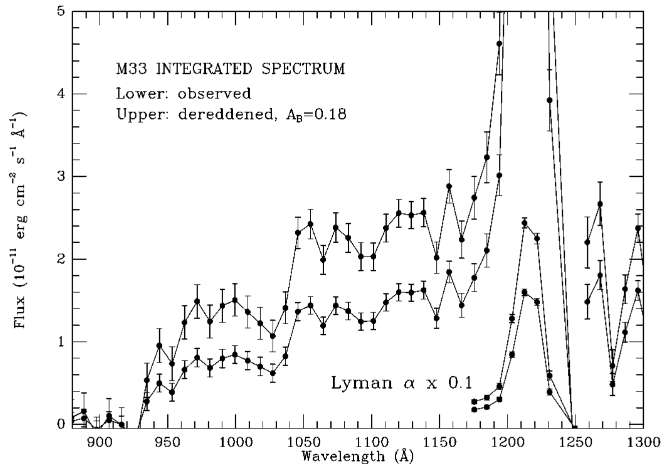

FIG. 3.—The integrated UVS spectrum of M33, plotted as observed and after correcting for foreground Galactic extinction. The Lyα region is overplotted at an intensity scale 10 times smaller. Error bars are $\pm 1\,\sigma$ from Poisson statistics of object plus background counts and should be reliable except with the Lyα line, where errors due to temporal changes in foreground emission dominate.

TABLE 1

M33 INTEGRATED SPECTRUM AND POISSON ERROR

λ (Å)	F_λ	σ_F
888.5	7.52E−13	1.06
897.7	−6.27E−13	1.05
907.0	5.05E−13	1.03
916.3	−2.47E−14	1.03
925.5	−1.81E−12	1.05
934.8	2.76E−12	1.07
944.0	4.98E−12	1.08
953.3	3.88E−12	1.08
962.6	6.61E−12	1.09
971.8	8.07E−12	1.10
981.1	6.84E−12	1.09
990.3	7.97E−12	1.10
999.6	8.45E−12	1.09
1008.9	7.72E−12	1.10
1018.1	7.00E−12	1.11
1027.4	6.18E−12	1.11
1036.6	8.24E−12	1.12
1045.9	1.36E−11	1.11
1055.2	1.44E−11	1.06
1064.4	1.19E−11	1.05
1073.7	1.43E−11	1.08
1082.9	1.37E−11	1.06
1092.2	1.24E−11	1.04
1101.5	1.25E−11	1.03
1110.7	1.47E−11	1.05
1120.0	1.59E−11	1.05
1129.2	1.59E−11	1.03
1138.5	1.62E−11	1.09
1147.8	1.28E−11	1.20
1157.0	1.84E−11	1.30
1166.3	1.44E−11	1.45
1175.5	1.77E−11	1.68
1184.8	2.10E−11	2.00
1194.1	3.01E−11	2.46
1203.3	8.44E−11	3.29
1212.6	1.59E−10	4.07
1221.8	1.48E−10	4.18
1231.1	3.92E−11	3.71
1258.9	1.48E−11	2.08
1268.1	1.80E−11	1.77
1277.4	4.82E−12	1.32
1286.7	1.11E−11	1.18
1295.9	1.62E−11	1.19

values certainly underestimate the extinction toward some parts of the H II regions; in our own vicinity, young clusters in, for example, Orion remain totally obscured in the optical. For UV radiation, stars that are significantly reddened optically will cease to be important contributors as long as some are almost unreddened (the "picket fence effect"). Hence, without external constraints on the total stellar population, any absolute extinction correction in the far-UV reflects more about the input assumptions than it does about the galaxy, while the spectral shape of the emerging radiation will be dominated by the least reddened stars, and this point is reflected in the data handling here.

2.2. *Comparison Data*

M33 has been widely observed across the electromagnetic spectrum, although modern observations are often limited by its large angular size. Several data sets have been matched to the UVS observing geometry, by masking regions beyond the bounds of the area observed, convolving with the appropriate resolution, and projecting along the axis of the UVS aperture.

Imaging from the Ultraviolet Imaging Telescope (UIT), conducted on the Astro-1 mission, has been reported by Landsman et al. (1992), in the 1500 and 2400 Å bands. They show evidence for a gradient in color between these wavelengths, perhaps most plausibly attributed to a radial change in the dust properties. The UIT images in filters A1 (1900–3000 Å) and B1 (1350–1700 Å) were retrieved from the National Space Science Data Center (NSSDC) for comparison with the *Voyager* measurements. Comparison of different exposures was used to reject glitches in individual images; a few bright foreground stars that are bright in the A1 filter but not at shorter wavelengths were also deleted from the images in order to avoid confusing the comparison with the deep-UV results. This was especially important for the bright star 69″ southeast of NGC 604, which is relatively blue by field standards but is dropping out by 1500 Å. The UIT images were rotated to match first the scan direction (enabling clipping of the small part of these images that is outside the UVS scan footprint) and then to match the aperture orientation of the UVS data in order to construct matching one-dimensional scans with the UVS spatial coverage. As it happens, both the UIT and *Voyager* observations truncate nearly the same area of the southernmost disk of M33, easing the comparison in this case. Still, an apparent flux decline at the eastern edge of the UIT slices results from the edge of the (circular) field, so that there is a region about 15′ wide with UVS signal lacking UIT coverage.

The core of NGC 604 was saturated in the longest UIT exposures; the effects of saturation were evaluated using the fluxes quoted from shorter exposures by Landsman et al. (1992) and the UIT images corrected by replacing the NGC 604 region with a Gaussian profile of the appropriate size and flux before block averaging to match the UVS sampling. As it happens, the flux correction due to this saturation is only a small fraction of the total as measured with the large aperture that is relevant for this comparison.

The total flux within each image (minus obvious foreground stars) was also extracted for comparison with the UVS data, yielding observed values of 1.95×10^{-11} ergs $cm^{-2}\ s^{-1}$ Å^{-1} at 1500 Å and 1.01×10^{-11} at 2400 Å. Background uncertainties contribute an error of about 8% at 2400 Å, while zero-point error is the dominant uncertainty at the shorter passband, since the sky is so dark that background errors contribute only 2%. For comparison, the integrated B and V magnitudes from the RC3 correspond to flux values of 2.25×10^{-11} at 4400 Å and 2.03×10^{-11} at 5500 Å. Like many star-forming galaxies, the integrated spectrum of M33 is nearly flat in F_λ across a wide wavelength range.

Several Hα surveys of M33 have been published. The best comparison for this purpose is with wide-field Hα data properly representing the diffuse emission. N. Devereux has made available a calibrated Hα image from the Burrell Schmidt telescope at Kitt Peak (Devereux, Duric, & Scowen 1997) that was averaged to an appropriate resolution and resampled to match the *Voyager* spectrometer scan. In matching the effective resolution, the response across the UVS aperture was taken as a Gaussian of FWHM = 6′.2, which is a very close approximation to the profile measured by scanning repeatedly across a star (Holberg & Watkins 1992).

3. M33 IN THE DEEP-ULTRAVIOLET

3.1. *The Continuum: Stellar Content*

A feature at about 1030 Å is prominent in O and B stars, due to a combination of Lyβ and O VI λλ1032, 1038 (e.g., Longo et al. 1989). González Delgado, Leitherer, & Heckman (1997) model this blend including Lyβ λ1032, O VI λλ1032, 1038, and C II λλ1036, 1037 Å. Unfortunately, they find that line profiles rather than equivalent widths are needed to distinguish the dominant contributors to the blend. This complex of lines is clearly seen in absorption in M33 with a collective equivalent width of 9 Å. An additional blend near 980 Å, consisting of Lyγ and C III λ977, was found by Longo et al. to be prominent in stars cooler than about B1, especially for luminosity classes III–V, and is also seen in M33, but the low spectral resolution and strong continuum slope make the strength of this absorption very uncertain.

Landsman et al. (1992) report an ultraviolet color gradient in M33, in the sense that the central region is redder between 1500 and 2400 Å. They attribute this to the distribution of dust within M33. The UVS data suggest that the effect continues into the deeper UV, showing evidence of a flatter distribution than that found from the UIT data even at 1500 Å (the far-UV passband of UIT filter B1). This may be seen from the profile comparison in Figure 4, showing the UV and Hα profiles at the same resolution and registration.

The spectrum of NGC 604 is of special interest, as it is one of the few local star-forming regions to be measured all the way to the Lyman limit. Sampled at the UVS spatial resolution, the UIT and Hα data show that it contributes 22%, 20%, and 39% of the total flux at its position as seen at 2500 and 1500 Å and at Hα, so that its signature will still appear with the UVS if its relative brightness is at the high end of this range. This is indeed the case, as is shown by the discrete peak in the continuum profile of M33 (Fig. 4), which would not appear if NGC 604 had the same 1000–1500 Å color as the galaxy disk. The UVS data do not have a secure coordinate zero point, so the combined registration of the nucleus and NGC 604 was used to align them with data from other passbands.

The slope of the current mass function and number of stars from spectral types A0–B0 can be estimated for M33

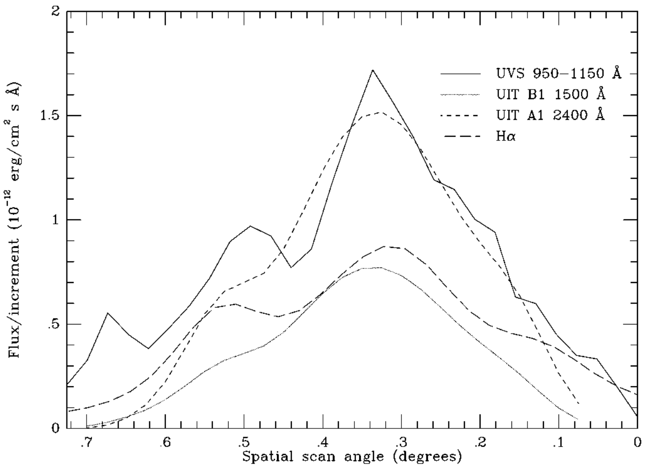

FIG. 4.—Spatial profile of M33 averaged between 950 and 1150 Å, compared with similarly averaged profiles at 1500 and 2400 Å from UIT data and in Hα. The giant H II region NGC 604 is increasingly prominent at shorter wavelengths and in Hα. Averaging over complex structure produces the shifts between Hα centroids at the nucleus and for NGC 604, for which the separation is consistent within the limits of this effect for all passbands. The three continuum traces have the same intensity scale, while the Hα trace has a peak value of 2.1×10^{-11} ergs cm^{-2} s^{-1} per resolution element. The apparent far-UV peak at a scan angle of 0°.72 is most likely spurious, resulting from counts in a single spatial increment, whereas NGC 604 affects the detected flux across three increments.

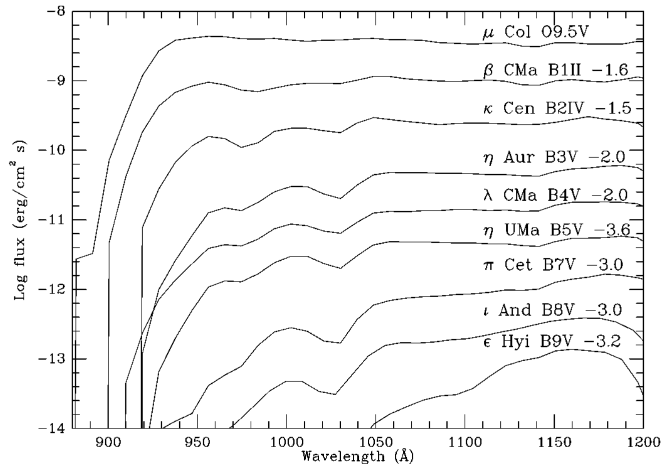

FIG. 5.—A sequence of hot stellar spectral standards observed with the *Voyager 1* and *2* UVS systems. For direct comparison with the M33 data, the *Voyager 1* observations have been interpolated to the wavelength bins of the *Voyager 2* instrument. Each star is labelled just above the long-wavelength end of its spectrum. Most stars have been scaled by the indicated amount in the logarithm for display; the fluxes at a reference wavelength of 1100 Å are listed in Table 2. The 980 and 1030 Å blends are prominent across much of this temperature range. For the hotter stars, artificial flux at the level of a few percent has been introduced shortward of the Lyman limits by the descattering procedure. The blueward wings of Lyα absorption appear for the later type stars. These data were provided by R. Polidan.

using the *Voyager* stellar library and assuming that these types of main-sequence stars dominate the 912–1200 Å light (more about this assumption shortly). Spectral standards spanning this type range are available from UVS observations (as described briefly by Evans, Holberg, & Polidan 1996). The stars used for this exercise are listed in Table 2 with the spectra shown in Figure 5. Note that β Canis Majoris was used after rescaling its luminosity to correspond to luminosity class V, in order to provide at least some coverage of this temperature range. *Hipparcos* parallaxes (ESA 1997) were used for their distances, giving 6 σ results even for the O9.5 star μ Col. These stars are all almost unreddened ($E_{B-V} < 0.05$) so that this source of uncertainty is minimized. The current mass function (the product of the initial mass function [IMF] and mass-lifetime relation) is approximated as a power law, $N(M)dM = M^{\alpha}dM$. As shown in Figure 6, the M33 spectrum is well fitted by $\alpha = -4.7 \pm 0.3$, which is closely consistent with simple expectations based on a Salpeter IMF and mass/luminosity ratio varying as $M^{-3.5}$. However, the interpretation of this fit is clouded by the role of evolved stars in this temperature range.

Massey et al. (1996) presented an optical spectroscopic survey of the brightest stars in M33 as detected in the UIT passbands, limited by FUV (1500 Å) flux. All the survey wavelengths, including the implicit optical selection for the spectral classification, favor luminous stars cooler than O stars. It is striking, as Massey et al. stress, that the identified UV-bright stars are dominated by evolved stars rather than the main sequence. From the data in their Table 1, *all* identified B stars in the uppermost 3.5 mag of the 1500 Å luminosity function are supergiants rather than class V stars. In this case, it still remains unclear what fraction of the deep-UV light can be attributed to main-sequence stars, given this dominance by a more evolved population (as discussed by, for example, Massey 1998). The 356 brightest UV objects (supergiants, W-R stars, and clusters) from their study account for a total 1500 Å flux of 1.4×10^{-12} ergs cm^{-2} s^{-1} Å^{-1} and a slightly greater total extrapolated to 1100 Å, which is about 10% of the total measured for the whole galaxy, so telling whether nonevolved stars are important in the integrated light will require substantially deeper surveys of UV-selected stars. As shown by González

TABLE 2

Voyager UVS STANDARD STARS

Star	Type	D (pc)	V	log F (1100 Å) (ergs cm^{-2} s^{-1} Å^{-1})	log L (1100 Å) (ergs s^{-1} Å^{-1})
μ Col........	O9.5	400	5.18	−8.47	34.81
β Cma	B1 II–III	153	1.98	−7.40	35.05
κ Cen	B2 IV	165	3.13	−8.11	34.41
η Aur	B3 V	67	3.18	−8.33	33.39
λ CMa	B4 V	124	4.47	−8.85	33.41
η UMa......	B5 V	31	1.85	−7.73	33.33
π Cet........	B7 V	135	4.24	−9.47	32.87
ι And........	B8 V	154	4.29	−9.91	32.54
ε Hyi........	B9 V	47	4.12	−10.47	31.00
α Lyr........	A0 V	7.8	0.03	−10.58	29.29

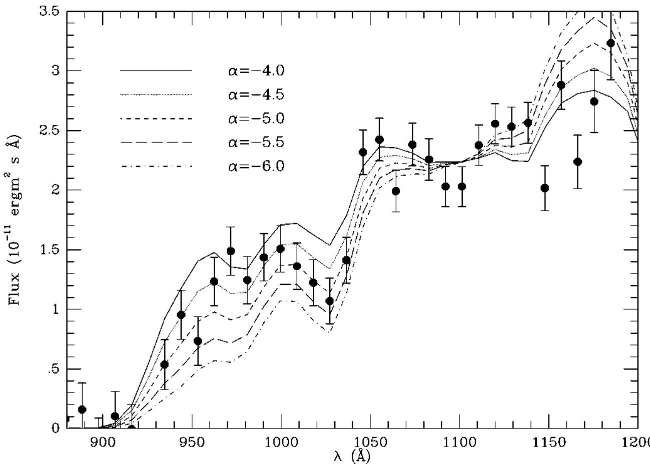

FIG. 6.—Schematic fitting of the current mass function to the dereddened M33 spectrum. The mass function is parameterized by $N(M) \propto M^{\alpha}$. The fits are produced by appropriate weighted mixes of the standard-star spectra normalized in the 1070–1130 Å region. The adopted best fit has $\alpha = -4.7 \pm 0.3$.

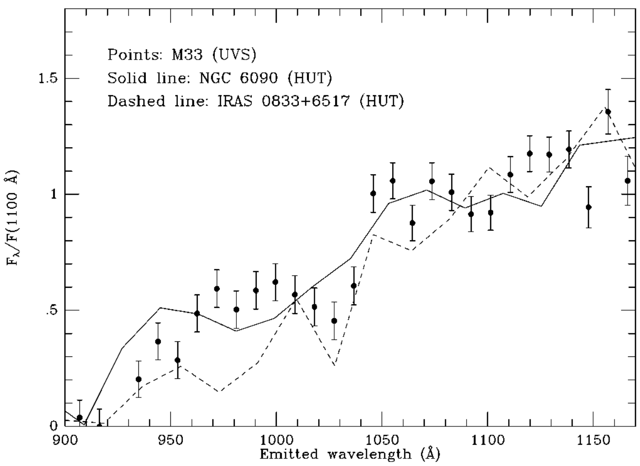

FIG. 7.—Comparison of the M33 integrated spectrum with the two starburst systems best observed by HUT in the same wavelength range, here plotted in the emitted frame for each object. The match in continuum shape is quite close, and the 1030 Å blend matches well with IRAS 0833+6517. For the HUT observations, pixels affected by geocoronal Lyα and Lyβ emission were clipped before averaging to the UVS resolution, which may contribute to the apparent variation in strength of the λ1030 feature.

Delgado et al. (1997), the spectral changes with luminosity in this wavelength range appear only at substantially higher spectral resolution.

The spectral fit shown in Figure 6 is therefore only illustrative and perhaps useful for prediction in observing high-redshift objects. A yet cruder but useful point of comparison is that the spectrum of a B4 star is a good first approximation to the M33 spectrum between 912–1200 Å; the power-law mass combinations do a better job, but for predicting fluxes the single-temperature approximation is within about 20% of the M33 spectrum at all wavelengths.

It is instructive to consider the M33 data in comparison with the Hopkins Ultraviolet Telescope (HUT) observations of starburst objects reported by Leitherer et al. (1995), especially as to continuum shape just longward of the Lyman limit. They used observations of four starburst systems with redshifts $cz > 5000$ km s^{-1}—IRAS 08339+6517, Mrk 1267, Mrk 66, and Mrk 496 (=NGC 6090)—to constrain the amount of intrinsic H I absorption at the Lyman edge. These galaxies, with high rates of star formation and short gas-consumption timescales, are a useful counterpoint to M33 with its more modest overall rate and, more importantly, its presumed history of a nearly constant disk star formation rate over long times. However, any differences in global spectra should be minor, since only the B-star population affects the deep ultraviolet, and the relative numbers of stars within this class could be modulated only briefly even by a very short burst. Figure 7 compares the dereddened M33 results with the two HUT observations having the highest signal-to-noise ratio, IRAS 08339+6517 and NGC 6090, omitting points affected by geocoronal Lyα and Lyβ emission, and rebinning the HUT data to approximately the UVS spectral resolution. The spectral shapes are quite comparable, with M33 roughly intermediate between the two starbursts for $\lambda < 1050$ Å. The 1030 Å blend is of nearly the same strength in M33 and IRAS 0833+6517, while it appears noticeably weaker in NGC 6090 (though it is possible that the measurement is somewhat corrupted by missing the spectral region that redshifts to geocoronal Lyβ). There is thus no indication here that the B-star population is substantially different in starbursts and in more normally star-forming galaxies; B stars are B stars across these global environments.

The spectrum must turn up below the Lyman limit, perhaps reflecting the temperature behavior of evolving massive stars. Using the integrated Hα flux of 4.4×10^{-10} ergs cm^{-2} s^{-1} and case B recombination, the mean flux from 700–900 Å should be of order 10^{-10} ergs cm^{-2} s^{-1} Å^{-1} under the usual assumption that the temperature distribution places most of the ionizing stellar photons within about 200 Å of the Lyman limit. The discrepancy is large enough that an upturn in F_λ must occur whatever the distribution of ionizing star temperatures. This exceeds the measured fluxes just longward of the Lyman limit by an order of magnitude. Even going to the deep ultraviolet, we are not seeing signatures of the most massive, ionizing stars. Note that this spectral upturn is deduced assuming that the same extinctions apply to O star light as derived from recombination lines and B stars from escaping UV radiation and could be relaxed if the typical extinction is small between O stars and the locations at which their ionizing radiation is transformed into longer wavelength emission lines.

3.2. *Lyα Emission*

As shown in Figures 2 and 3, Lyα emission is clearly detected in M33 even after making the large corrections for emission from the interplanetary medium and backscattered solar emission. The line has an integrated flux of $1.8 \pm 0.4 \times 10^{-9}$ ergs cm^{-2} s^{-1} as observed, corresponding to 2.3 ± 0.6 after correction for foreground reddening. This gives an equivalent width of 105 Å against the local continuum and a Lyα/Hα ratio in the range 3–5, ignoring any corrections for internal reddening in M33 (which would be very difficult to assess in any case because of the complex interplay between scattering and absorption for Lyα). The true ratio may be even larger because of Lyα absorption in our own interstellar medium.

The radial velocity range of M33 just misses overlap with the velocities of foreground H I. As shown by Deul & van der Hulst (1987), H I emission from the disk of M33 ranges from -300 to -70 km s^{-1}, which is in contrast to the foreground emission that is at positive velocities in this Galactic quadrant ($l = 133°.7$, $b = -31°.6$). However, the strong Lyα absorption associated with the foreground gas is a serious concern and poses a bit of a paradox. The mean foreground H I column density (using the surveys summarized by Dickey & Lockman 1990 and extracted using SkyView) is 5.3×10^{20} cm^{-2}. At these column densities, virtually all the emission from M33 would fall in high-opacity parts of the absorption profile, but the UVS data seem quite clear that emission is detected; using the profile form given by Bohlin (1975) for the damping wings, the absorption would be virtually complete for all M33 velocities at the mean column density and a small effect for most velocities at a tenth of this value. The situation is similar to the poor correlation found between H I emission and Lyα absorption measures of column density when only emission data of poor angular resolution were available. The detection of emission from Lyα probably means that fine structure in our own interstellar medium creates a mismatch between the mean opacities as measured in emission and absorption through clumpiness or patchiness. This further suggests that the Lyα intensity found here is likely to be a lower limit.

Figure 2 compares the spatial profiles of net Lyα emission and the continuum from 950–1150 Å. The line emission is more diffuse than the continuum and in particular shows no evidence for Lyα at the position of NGC 604, which remains prominent in the deep-UV continuum. Specifically, an upper limit on Lyα must be about 20% of the total, or 3.6×10^{-10} ergs cm^{-2} s^{-1} (regardless of details of the foreground correction from He I emission) for the position including NGC 604. Otherwise, the profile resembles that of the diffuse Hα emission without the giant H II regions. It is tempting to speculate that the diffuse ISM in spiral galaxies is a much more appealing source for escaping Lyα photons than are individual, luminous H II regions. In some cases, the diffuse ISM seems to have a velocity structure that might allow the line photons to be shifted outside the absorption core before many scatterings have occurred. If this is the case, even if the ionizing photons originated in H II regions, much of the Lyα would come from areas at a significant distance from their origin. This is consistent with the results of *HST* spectroscopy in nearby star-forming galaxies, which fail to show any consistent pattern between Lyα emission and either metallicity or local velocity width (as noted by Thuan & Izotov 1997).

A role for the diffuse ISM in the escape of Lyα implies that the line emission should be stronger for large apertures rather than for measurements encompassing individual star-forming regions. This certainly applies to spectra of objects currently being found at $z > 2$. As another local comparison system observed with a large enough aperture to encompass the whole galaxy, one may consider the interacting starburst system Mrk 357. There is an archival *IUE* spectrum (SWP 45198) with 25,800 s exposure, obtained in 1992 by M. Shull, shown in Figure 8. At its redshift of $z = 0.053$, Lyα is well separated from geocoronal emission and can be clearly seen with an equivalent width in the range 10–13 Å and flux 1.4–1.9 $\times 10^{-13}$ ergs cm^{-2} s^{-1} and marginal evidence for absorption on the blue side of the line. An Hα measurement is available from the intensified image dissector scanner system at the KPNO 2.1 m telescope with its flux scale confirmed via precise photoelectric *BV* photometry. This yields $F(\mathrm{H}\alpha) = 5.22 \times 10^{-13}$ ergs cm^{-2} s^{-1} and, after correcting for foreground reddening of $A_B = 0.17$, a flux ratio of Lyα/Hα = 0.43. The effects of internal reddening on the Balmer decrement are modest in this case, where the Hα/Hβ flux ratio is 4.05. This system is certainly luminous enough to find at high redshifts, and its optical line ratios indicate a substantial metallicity, providing further direct and local evidence that star-forming galaxies can have significant Lyα emission. While the literature has included contradictory claims on this point, observations of other nearby star-forming galaxies (such as blue compacts) have indicated this for some time.

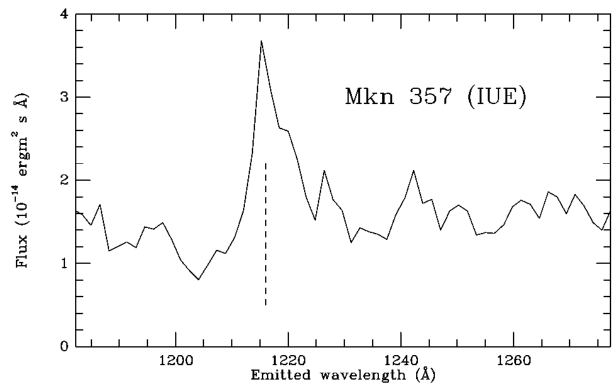

FIG. 8.—Lyα emission in the starburst system Mrk 357 at $z = 0.053$, from a long *IUE* short-wavelength prime camera exposure (No. 45,198). The dashed line shows the nominal location of Lyα based on the redshifts of optical emission lines.

4. CONCLUSIONS

An archival *Voyager 2* deep-ultraviolet observation of M33 has been analyzed to shed light on the line and continuum properties of a well-understood nearby galaxy at very short wavelengths. The continuum shows features from B stars and can be well fitted by a typical mix of B-type stellar templates, though the role of evolved stars means that the significance of such a fit is reduced. The spectrum from 912–1200 Å is very similar to that of two starburst galaxies observed by HUT; the hot-star populations are evidently similar in kind and different only in number.

Lyα emission is detected from the disk of M33 but apparently not from the giant H II region NGC 604 despite its strong continuum flux down to the Lyman limit. This may suggest that the diffuse ISM, rather than H II regions directly, is the dominant source for escaping Lyα photons on galactic scales. This suggestion may be tested by observing Lyα in galaxies with a significant diffuse emission-line component at redshifts just large enough that the details of Galactic H I absorption are not important. For much of the sky, this is satisfied for $z > 0.008$.

The properties of M33 are of special interest in comparison with star-forming objects now being observed, mostly in the deep emitted-UV, at large redshifts. For this comparison, the Cepheid distance of 840 kpc (Freedman, Wilson, & Madore 1991) is taken. M33 has a Lyα luminosity of at least 4.5×10^{45} ergs s^{-1} and a continuum luminosity at 1100 Å of about 1.8×10^{39} ergs s^{-1} Å^{-1}. For comparison with several grouping of galaxies recently observed at $z = 2.3$–2.5, I evaluate the fluxes that would be observed placing M33 at $z = 2.4$. Considering the range of "plausible" cosmologies with $q_0 = 0.1$–0.5 and $H_0 = 50$–100 km s^{-1} Mpc^{-1}, M33 at its measured Lyα luminosity would have a line flux of $2 \times 10^{-18} - 3 \times 10^{-17}$ ergs cm^{-2} s^{-1}, with the value 2×10^{-17} for a reference combination of $H_0 = 80$, $q_0 = 0.5$. The emission-line objects reported by Pascarelle et al. (1996), omitting three with spectroscopically obvious active nuclei, have observed Lyα fluxes in the range 10^{-17}–10^{-16}: that is, any object with the emission-line luminosity of M33 would be just at the limit of straightforward detection with current imaging narrow band, either from *HST* or the ground, at $z = 2.4$. The comparison is even more one-sided when the linear sizes are included; Lyα and Hα are strong over a region almost 1° across (roughly 15 kpc), so the line emission from M33 would extend over many times the sizes of most of the high-redshift emitters (some of which have effective radii as small as 0″.1, as found by Pascarelle et al. and presumably in many of the blue compact objects found in the Hubble Deep Field by Lowenthal et al. 1997). This emission-line extent, in contrast, maps to 1″.3–5″.3 for the plausible range of cosmologies, with a diameter of 4″.2 in the reference case. As found for the 1500 Å continuum by Giavalisco et al. (1996b), the line emission from galaxies like M33 is both too faint and too diffuse for current detection at high redshifts, making the objects that have been found stand out even more relative to nearby objects. Some of the smallest high-redshift objects are similar in emission-line extent to supergiant H II regions but are clearly far more luminous as Lyα sources (since NGC 604 is not even detected in M33). However, the M33 data do bode well for further use of Lyα at high redshifts, showing that the line can be detectable in galaxies with nontrivial metallicity, so that the high-redshift detections in ostensibly star-forming galaxies (as distinct from active galactic nuclei) are reasonable. Clearly, the role of ISM structure seen in nearby objects shows that Lyα is not always strong in star-forming objects, but it is now clear that it *may* be, offering a potentially useful probe of the star formation and ISM at early epochs, as well as a convenient discovery tool at large redshifts.

Special thanks to J. Holberg and J. Collins for help with the UVS archive and to whoever suggested this observation (which was done before I started graduate school); I regret being unable to determine who this was. The reduction visit to Arizona was partially supported by an EPSCoR grant. Presentation of this work was supported by NASA ADP grant NAG 5-3402. R. Polidan supplied the *Voyager* UVS spectra of hot Galactic stars. N. Devereux provided his wide-field Hα data in advance of publication. C. Leitherer provided his HUT spectra via the World Wide Web for comparison. Figure 1 uses data from the Digitized Sky Survey, which is based on photographic data obtained using the Oschin Schmidt Telescope on Palomar Mountain. The Palomar Observatory Sky Survey was funded by the National Geographic Society. The Oschin Schmidt Telescope is operated by the California Institute of Technology and Palomar Observatory. The plates were processed into the present compressed digital format with their permission. The Digitized Sky Survey was produced at the Space Telescope Science Institute under U. S. government grant NAG W-2166. The foreground H I data were extracted using the SkyView facility at Goddard Space Flight Center.

REFERENCES

Bohlin, R. C. 1975, ApJ, 200, 402
Bonilha, J. R. M., Ferch, R., Salpeter, E. E., Slater, G., & Noerdlinger, P. D. 1979, ApJ, 233, 649
Broadfoot, A. L., et al. 1977, Space Sci. Rev., 21, 183
Deul, E. R., & van der Hulst, J. M. 1987, A&AS, 67, 509
de Vaucouleurs, G., et al. 1991, Third Reference Catalog of Bright Galaxies (Berlin: Springer) (RC3)
Devereux, N., Duric, N., & Scowen, P. A. 1997, AJ, 113, 236
Díaz, A. I., Terlevich, E., Pagel, B. E. J., Vilchez, J. M., & Edmunds, M. G. 1987, MNRAS, 226, 19
Dickey, J. M., & Lockman, F. J. 1990, ARA&A, 28, 215
ESA, 1997, *Hipparcos* and *Tycho* Catalogues (ESA SP-1200) (Noordwijk: ESA)
Evans, N. R., Holberg, J. B., & Polidan, R. S. 1996, AJ, 112, 264
Freedman, W. L., Wilson, C. D., & Madore, B. F. 1991, ApJ, 372, 455
Giavalisco, M., Koratkar, A., & Calzetti, D. 1996a, ApJ, 466, 831
Giavalisco, M., Livio, M., Bohlin, R. C., Macchetto, F. D., & Stecher, T. P. 1996b, AJ, 112, 369
González Delgado, R. M., Leitherer, C., & Heckman, T. 1997, ApJ, 489, 601
Hartmann, L. W., Huchra, J. P., Geller, M. J., O'Brien, P., & Wilson, R. 1988, ApJ, 326, 101
Holberg, J. B., & Watkins, R. 1992, *Voyager* Ultraviolet Spectrometer Guest Observer and Data Analysis Handbook (Tucson: Lunar and Planetary Lab.)
Johnson, S. B., & Joner, M. D. 1987, AJ, 94, 324
Kunth, D., Lequeux, J., Sargent, W. L. W., & Viallefond, F. 1994, A&A, 282, 709
Landsman, W. B., Roberts, M. S., Bohlin, R. C., O'Connell, R. W., Smith, A. M., & Stecher, T. P. 1992, ApJ, 401, L83
Leitherer, C., Ferguson, H. C., Heckman, T. M., & Lowenthal, J. D. 1995, ApJ, 454, L19
Lequeux, J., Kunth, D., Mas-Hesse, J. M., & Sargent, W. L. W. 1995, A&A, 301, 18
Longo, G., Stalio, R., Polidan, R. S., & Rossi, L. 1989, ApJ, 339, 474
Lowenthal, J. D., Koo, D. C., Guzman, R., Gallego, J., Phillips, A. C., Faber, S. M., Vogt, N. P., Illingworth, G. D., & Gronwall, C. 1997, ApJ, 481, 673
Massey, P. 1998, in Stellar Initial Mass Function, Proc. 38th Herstmonceux Conf., ed. G. Gilmore, I. Perry & S. Ryan (San Francisco: ASP), in press
Massey, P., Bianchi, L., Hutchings, J. B., & Stecher, T. B. 1996, ApJ, 469, 629
McCall, M. L., Rybski, P. M., & Shields, G. A. 1985, ApJS, 57, 1
Pascarelle, S. M., Windhorst, R. A., Keel, W. C., & Odewahn, S. C. 1996, Nature, 383, 45
Sandel, B. R., Shemansky, D. E., & Broadfoot, A. L. 1978, Nature, 274, 666
Savage, B. D., & Mathis, J. S. 1979, ARA&A, 17, 73
Shemansky, D. E., Sandel, B. R., & Broadfoot, A. L. 1979, J. Geophys. Res., 84, 139
Snow, T. P., Allen, M. M., & Polidan, R. S. 1990, ApJ, 359, L23
Steidel, C. C., Adelberger, K. L., Dickinson, M., Giavalisco, M., Pettini, M., & Kellogg, M. 1998, ApJ, 492, 428
Steidel, C. C., Giavalisco, M., Dickinson, M., & Adelberger, K. L. 1996b, AJ, 112, 352
Steidel, C. C., Giavalisco, M., Pettini, M., Dickinson, M., & Adelberger, K. L. 1996a, ApJ, 462, L17
Thuan, T. X., & Izotov, Y. I. 1997, ApJ, 489, 623